Energy & Environmental Science

RSC Publishing

PAPER

Postsynthetic tuning of hydrophilicity in pyrazolate MOFs to modulate water adsorption properties†

Cite this: *Energy Environ. Sci.*, 2013, **6**, 2172

Casey R. Wade, Tachmajal Corrales-Sanchez, Tarun C. Narayan and Mircea Dincă*

Metal–organic frameworks (MOFs) have attracted interest as adsorbents in water-based adsorption heat pumps owing to their potential for increased water loading capacities and structural and functional tunability *versus* traditionally used materials such as zeolites and silica. Although pyrazolate-based MOFs exhibit exceptional hydrolytic stability, the water adsorption characteristics of this class of frameworks have remained unexplored in this context. In this report, we describe the modular synthesis of novel dipyrazole ligands containing naphthalenediimide cores functionalized with –H (H_2NDI–H), –NHEt (H_2NDI–NHEt), or –SEt (H_2NDI–SEt) groups. Reaction of these ligands with $Zn(NO_3)_2$ afforded an isostructural series of MOFs, Zn(NDI–X), featuring infinite chains of tetrahedral Zn^{2+} ions bridged by pyrazolate groups and ~16 Å-wide channels with functionalized naphthalenediimide linkers lining the channel surface. The Type V water adsorption isotherms measured for these materials show water uptake in the 40–50% relative humidity range, suggesting hydrophobic channel interiors. Postsynthetic oxidation of Zn(NDI–SEt) with dimethyldioxirane was used to generate ethyl sulfoxide and ethyl sulfone groups, thereby rendering the channels more hydrophilic, as evidenced by shifts in water uptake to the 30–40% relative humidity range. Such tunability in water adsorption characteristics may find utility in the design of new adsorbents for adsorption-based heat transfer processes. An original MATLAB script, MOF-FIT, which allows for visual modeling of breathing and other structural deformations in MOFs is also presented.

Received 13th March 2013
Accepted 13th May 2013

DOI: 10.1039/c3ee40876k

www.rsc.org/ees

Broader context

The transfer of heat *via* adsorption/desorption of various gases or vapors by porous materials has long been recognized for potential applications in heat storage and transformation. The possible benefits of adsorption-based heat pump systems include the ability to utilize low temperature waste heat and/or solar thermal energy and use of environmentally benign working fluids such as water. Porous materials such as silica and zeolites have traditionally been studied as adsorbents in water-based adsorption heat pump applications. However, these materials suffer from a lack of structural and functional tunability, hindering modulation of hydrophilicity and water exchange capacity which directly correlate to their efficiency in water adsorption-based applications. Recently, a new class of porous hybrid materials, metal–organic frameworks (MOFs), has emerged which allow for unprecedented control over structure and chemical functionality. In this study, we describe the use of a simple postsynthetic modification strategy to control the hydrophilicity and water vapor adsorption properties of a new set of water stable Zn^{2+}–pyrazolate MOFs. This postsynthetic modification strategy, along with a scalable, modular ligand synthesis, represent promising new approaches for the design of water sorption materials with tunable hydrophilicity and applications in energy efficient and environmentally friendly adsorption heat pump devices.

Introduction

Adsorptive heat transformations are environmentally friendly and energy-efficient means of heating and cooling. Unlike traditional vapor-compression heat pumps which rely entirely on electrical power, adsorption-based processes can exploit low-temperature waste heat or solar collectors as primary energy sources.[1–3] A general cycle for the operation of an intermittent adsorption cooling process is shown in Fig. 1. In the working cycle, evaporation of a fluid, such as water, produces desired cooling in the application environment while adsorption of the working fluid vapors at the adsorbent releases heat into an external environment. Regeneration of the adsorbent is then carried out with low temperature waste or solar heat to complete the cycle. While a number of working fluids could be employed, water is the most economically viable and environmentally benign option, and porous materials such as silicas and zeolites have been examined as complementary adsorbents.[4–12] Silicas generally display poor water exchange capacities, in part due to their low hydrophilicity. Water exchange capacity, the amount of water adsorbed and desorbed per gram adsorbent during the

Department of Chemistry, Massachusetts Institute of Technology, Cambridge, MA 02139, USA. E-mail: mdinca@mit.edu

† Electronic supplementary information (ESI) available: Script files, documentation, and example input files for MOF-FIT (MATLAB files). Synthetic and experimental details, PXRD and TGA data, NMR and IR spectra. See DOI: 10.1039/c3ee40876k

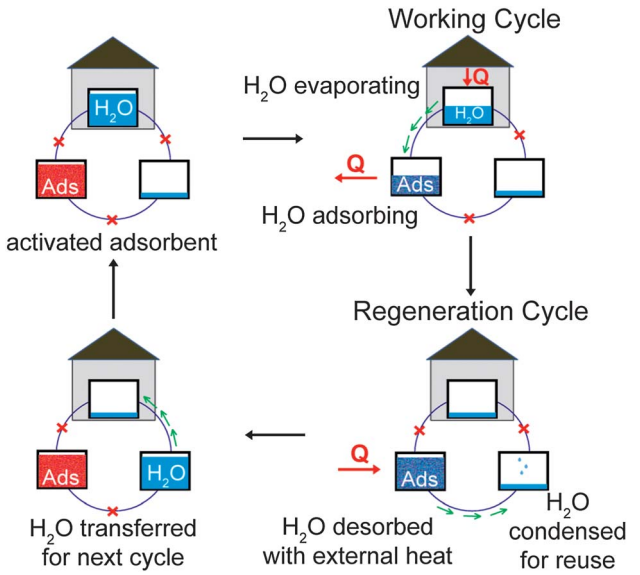

Fig. 1 Diagram of an intermittent adsorption cooling process.

working and regeneration cycles, is a key criterion since it ultimately dictates the amount of heat transferred in a given cycle. More hydrophilic zeolites and zeolite-type materials have been shown to exhibit increased water exchange capacities, but the increase in hydrophilicity leads to higher desorption temperatures which may surpass those provided by low-temperature waste heat or solar collectors. More recently, metal–organic frameworks (MOFs) have attracted interest as adsorbents in water-based adsorption heat pumps primarily owing to their potential for increased water loading capacities, which may exceed 1 g H_2O per g adsorbent. In contrast, silicas and zeolites typically achieve loadings of only 0.2–0.4 g H_2O per g adsorbent.[11,12] Equally attractive is the ability to control structure and functionality within MOF materials *via* the inorganic and organic building blocks. This feature should allow for tuning of properties such as enthalpy of adsorption and relative humidity and temperature at which adsorption/desorption occurs, factors which dictate the suitability of the sorbent to specific adsorption heating/cooling applications.

While much effort has been placed toward tuning the structure and function of MOFs for adsorption and separation of gases such as H_2, CH_4, and CO_2, less attention has been given toward modifying their water adsorption properties.[13–15] This is due, at least in part, to the hydrolytic instability of many MOFs.[16–19] Nonetheless, the water adsorption behaviors of the few water-stable, *carboxylate*-based MOFs such as MIL-101(Cr) and MIL-100(Fe) have been studied in some detail and evidenced characteristics desirable in heat pump adsorbents.[12,16,20–24] Despite reports of exceptional water stability, water adsorption isotherms have not been measured for *pyrazolate*-based MOFs.[25] Herein we report the synthesis and water adsorption properties of a series of Zn–pyrazolate frameworks based on dipyrazole ligands containing functionalized naphthalenediimide cores. We show that the humidity range for water uptake depends largely on the hydrophobicity of the pore surface, and that the latter can be modified postsynthetically to easily tune MOF materials for water sorption devices.

Results and discussion

To avoid arduous synthetic pathways commonly used to obtain dipyrazole ligands, we have employed a modular synthesis involving the condensation of 4-amino-3,5-dimethylpyrazole with linear arene dianhydrides.[26] This route allows for multigram scale synthesis of dipyrazole ligands from commercially available precursors as well as facile access to functionalized derivatives. The new dipyrazole ligand H_2NDI–H was synthesized by condensation of 2 equivalents of 4-amino-3,5-dimethylpyrazole with naphthalene dianhydride in DMF (Scheme 1). Subsequent reaction of H_2NDI–H with $Zn(NO_3)_2 \cdot 6H_2O$ in *N*,*N*-dimethylformamide (DMF) at 130 °C afforded Zn(NDI–H) as a microcrystalline yellow powder. The powder X-ray diffraction (PXRD) pattern of Zn(NDI–H) closely matched a pattern simulated from a structural model based on Co(dmdpb) (dmdpb = 1,4-bis[(3,5-dimethyl)dipyrazol-4-ylbenzene), suggesting a common structure type consisting of infinite chains of tetrahedral Zn^{2+} ions bridged by pyrazolate groups.[25,27–30] However, breathing distortions in which variation in the angle (θ) made between two ligands at a metal node results in oblique rather than square channels are known to occur in dipyrazolate-based MOFs.[27,30,31] To model this type of distortion, we have developed an original visual fitting routine, MOF-FIT, implemented in MATLAB, which allows determination of breathing angles and other translational MOF deformations by dynamically simulating structures with varying θ input angles and visually comparing the results in calculated and experimental PXRD patterns (see ESI for script files and step-by-step instructions for this general routine†). Using this method, we found that the experimental pattern of Zn(NDI–H) more closely matched that of a model structure with a breathing angle (θ) of 77° rather than 90° (Fig. 2). The simulated structure indicates that Zn(NDI–H) contains ~16 Å-wide channels with naphthalenediimide linker groups lining the channel surface.

In agreement with the expected microporous structure, thermogravimetric analysis (TGA) showed the loss of ~4 DMF guest solvent molecules per formula unit upon heating to 140 °C and a subsequent mass loss occurring at ~500 °C, likely indicative of decomposition of the framework (Fig. S1†). An apparent Brunauer–Emmett–Teller (BET) surface area of 1460 $m^2\ g^{-1}$ was calculated from a N_2 adsorption isotherm

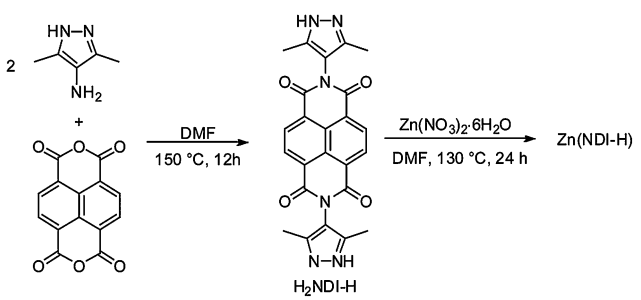

Scheme 1 Synthesis of H_2NDI–H and Zn(NDI–H).

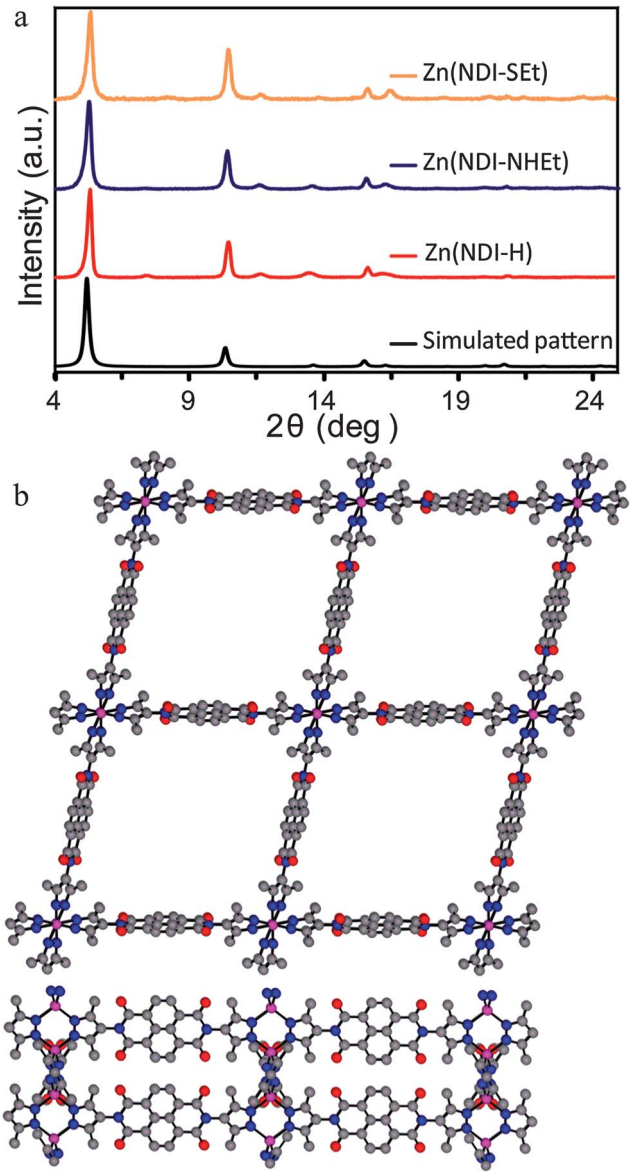

Fig. 2 (a) Powder X-ray diffraction patterns of Zn(NDI–X) (X = H, NHEt, SEt). (b) Simulated structure of Zn(NDI–H).

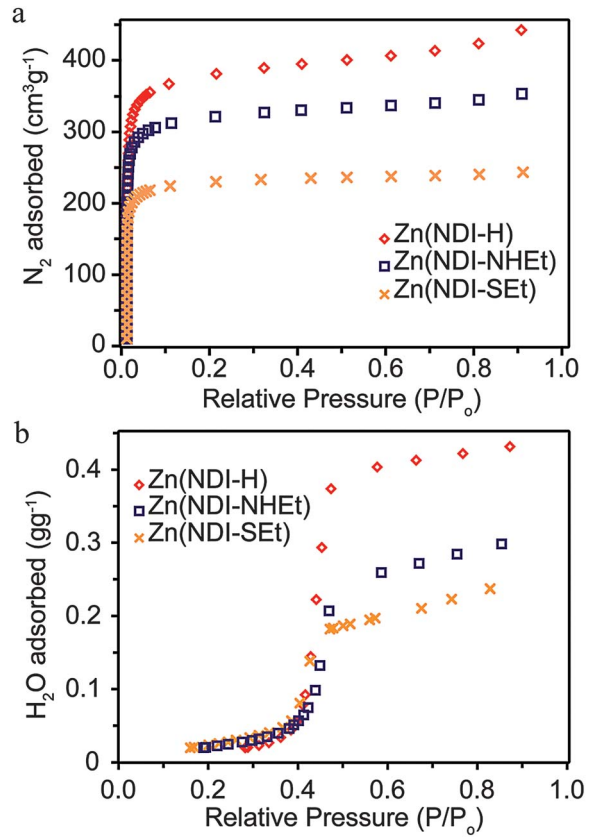

Fig. 3 (a) N_2 and (b) H_2O adsorption isotherms for Zn(NDI–H), Zn(NDI–NHEt), and Zn(NDI–SEt) measured at 77 K and 293 K, respectively.

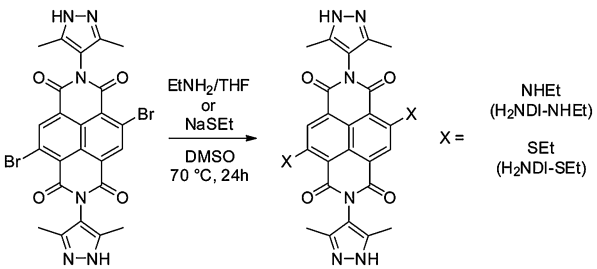

Scheme 2 Synthesis of H_2NDI–EtNH and H_2NDI–SEt.

measured at 77 K on a sample of Zn(NDI–H) activated by heating in vacuum (10^{-4} to 10^{-5} torr) at 160 °C for 24 h (Fig. 3a). In line with the exceptional hydrolytic stability observed for other pyrazolate-based MOFs, no significant changes were observed in the PXRD pattern of Zn(NDI–H) after immersion in water for 24 h (Fig. S2†).

We considered that modification of the naphthalene core of the dipyrazole ligands in Zn(NDI–H) could provide a convenient means to study the effects of pore hydrophilicity on the water adsorption characteristics of pyrazolate-based MOFs. Conveniently, nucleophilic aromatic substitution of core-halogenated NDIs has been used to install a variety of functional groups at the naphthalene core.[32] Thus, we synthesized the dibrominated dipyrazole H_2NDI–Br and found that it reacts cleanly with $EtNH_2$ and Na(SEt) to generate the new dipyrazole ligands H_2NDI–NHEt and H_2NDI–SEt, respectively (Scheme 2). Subsequent reaction of H_2NDI–NHEt and H_2NDI–SEt with $Zn(NO_3)_2 \cdot 6H_2O$ in DMF at 130 °C afforded Zn(NDI–NHEt) and Zn(NDI–SEt) as blue and red/orange microcrystalline powders, respectively. PXRD analysis of Zn(NDI–NHEt) and Zn(NDI–SEt) confirmed their isostructural relationship with Zn(NDI–H) (Fig. 2a). The TGA profiles of Zn(NDI–NHEt) and Zn(NDI–SEt) showed the loss of DMF guest solvent molecules up to 140 °C and the apparent onset of decomposition at around 450 °C and 350 °C, respectively (Fig. S3 and S4†). N_2 adsorption isotherms measured at 77 K on samples of Zn(NDI–NHEt) and Zn(NDI–SEt) activated by heating in vacuum at 140 °C for 24 h gave apparent BET surface areas of 1236 $m^2\ g^{-1}$ and 888 $m^2\ g^{-1}$, respectively (Fig. 3a). The lower values observed for these relative to Zn(NDI–H) may be attributed to the functional groups that partially block the pores of the substituted materials.[33,34]

The volumetric water adsorption isotherms for evacuated samples of Zn(NDI–H), Zn(NDI–NHEt), and Zn(NDI–SEt) were measured at 293 K and are shown in Fig. 3b. These materials all exhibit Type V isotherms and show little water adsorption over the relative humidity range P/P_o = 0–0.4, but experience sharp increases in water uptake at P/P_o = 0.4–0.5 (~6.9 to 8.7 torr).[35] This behavior is similar to that observed for water adsorption in activated carbons and suggests largely hydrophobic character for the interior surface of the MOF channels.[36,37] More notably, these observations are in agreement with the similarity of the hydrophobic parameters (π) for the ligand substituents –H (0.00), –NHEt (+0.08), and –SEt (+1.07) exposed at the MOF channel surface.[38]

In light of these results, we sought a means to more drastically alter the hydrophilicity of the functional groups decorating the channel interior and examine the ensuing effects on the water adsorption step. Consequently, we attempted postsynthetic oxidation of the sulfide groups decorating the channel interior of Zn(NDI–SEt) to generate more polar and hydrophilic sulfoxide (–SOEt, π = −1.04) and sulfone (–SO_2Et, π = −1.09) groups. Treatment of red-orange suspensions of Zn(NDI–SEt) in acetone with either 2 eq. or 8 eq. of dimethyldioxirane at −20 °C resulted in gradual color changes to afford orange-yellow Zn(NDI–SOEt) and yellow Zn(NDI–SO_2Et), respectively.[39] After filtration and washing with fresh acetone, powder X-ray diffraction confirmed that the crystallinity of both samples was retained without any significant structural changes (Fig. S5†). The IR spectrum of Zn(NDI–SOEt) showed the appearance of two new bands: a strong band at 1047 cm^{-1} and a weak band at 1136 cm^{-1}, corresponding to the formation of sulfoxide and sulfone groups, respectively (Fig. S6†). The IR spectrum of Zn(NDI–SO_2Et) displayed an intense new signal at 1136 cm^{-1}, suggesting the predominant conversion of the sulfide groups to sulfones. The ^{1}H NMR spectra of samples of Zn(NDI–SOEt) and Zn(NDI–SO_2Et) digested in mixtures of DMSO-d_6, DCl, and D_2O were measured to quantify the degree of oxidation of the sulfide groups and are shown in Fig. 4. The spectrum of Zn(NDI–SOEt) showed a mixture of products in the ratio 1 : 8 : 1 sulfide : sulfoxide : sulfone while that of Zn(NDI–SO_2Et) indicated nearly complete oxidation of the sulfide to give a 2 : 8 sulfoxide : sulfone mixture.

The TGA profile of Zn(NDI–SOEt) showed two distinct mass losses up to 180 °C, with continuing gradual decrease in mass up to the apparent framework decomposition at around 500 °C while that of Zn(NDI–SO_2Et) exhibited loss of guest solvent molecules up to 115 °C and the apparent onset of framework decomposition around 350 °C (Fig. S7 and S8†). Samples of Zn(NDI–SOEt) and Zn(NDI–SO_2Et) activated at 50 °C and 100 °C under vacuum exhibited apparent BET surface areas of 927 m^2 g^{-1} and 764 m^2 g^{-1}, respectively (Fig. 5a), in line with that of Zn(NDI–SEt) (888 m^2 g^{-1}).[40] PXRD analysis of these samples after activation indicated that bulk crystallinity was maintained while the ^{1}H NMR spectra of acid-digested samples showed retention of the sulfoxide and sulfone functionalities (Fig. S9 and S10†).

Remarkably, the water uptake steps of the adsorption isotherms for activated samples of Zn(NDI–SOEt) and Zn(NDI–SO_2Et), shown in Fig. 5b along with Zn(NDI–SEt) for comparison, are shifted to lower relative humidity of around P/P_o = 0.2–0.3 (~3.5–5.2 torr) for Zn(NDI–SOEt) and 0.3–0.4 (~5.2–7.0 torr) for Zn(NDI–SO_2Et). While these shifts are in agreement with the greater hydrophilicity of the –SOEt and –SO_2Et groups *versus* –SEt, the water adsorption step for Zn(NDI–SOEt) is clearly shifted from that of Zn(NDI–SO_2Et) despite similar hydrophobic parameters for the –SOEt (−1.04) and –SO_2Et (−1.09) groups. However, these hydrophobic parameters, derived from water–octanol partitioning, differ from hydrophilicity data determined in other solvent mixtures. Namely, partition coefficients determined from water–alkane mixtures (log P_{alk}) for methyl phenyl sulfoxide (log P_{alk} = −1.52) and methyl phenyl sulfone (log P_{alk} = −0.87) suggest that sulfoxides exhibit greater hydrophilic character than sulfones in highly hydrophobic environments.[41,42] This behavior corroborates the larger shift observed for the water adsorption step of Zn(NDI–SOEt) *versus* Zn(NDI–SO_2Et) given the otherwise hydrophobic character of the MOF channel interior.

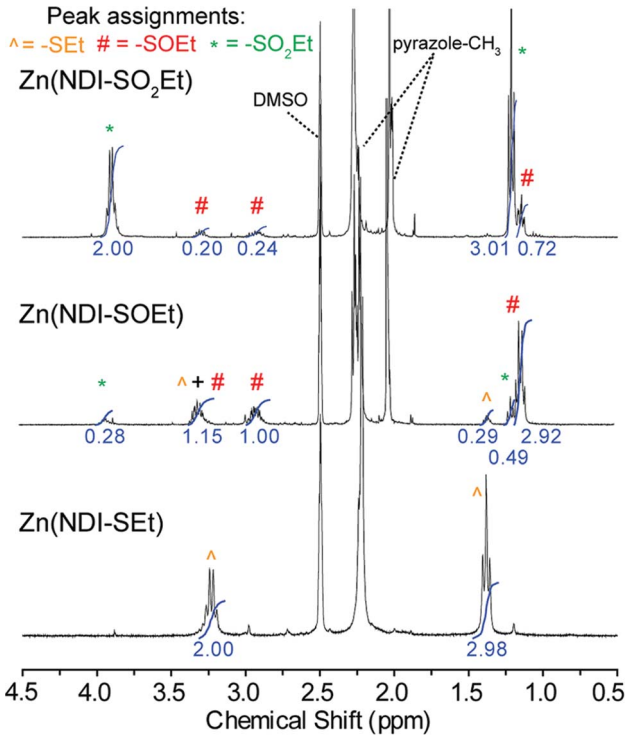

Fig. 4 ^{1}H NMR spectra of samples of Zn(NDI–SOEt) and Zn(NDI–SO_2Et) digested with DMSO-d_6/DCl/D_2O.

The oxidation-induced shifts in the water adsorption steps of Zn(NDI–SOEt) and Zn(NDI–SO_2Et) *versus* Zn(NDI–SEt) demonstrate the potential for MOF adsorbents to be tuned for water sorption cooling applications. In the working cycle of an adsorption chiller, heat is transferred by the evaporation of water at a cooling application temperature (T_{evap}) and the adsorption of water by the adsorbent at a temperature (T_{ads}). In order to realize efficient cooling to a desired T_{evap}, the adsorbent should be capable of reaching a high water loading at a relative humidity, (P/P_o), less than or equal to $P_{evap}/P_{sat}(T_{ads})$, where $P_{sat}(T_{ads})$ is the saturation pressure corresponding to a temperature of T_{ads}. This condition depends on both the adsorbent temperature T_{ads} and the intrinsic water adsorption profile of the adsorbent. Therefore, the relative humidity at

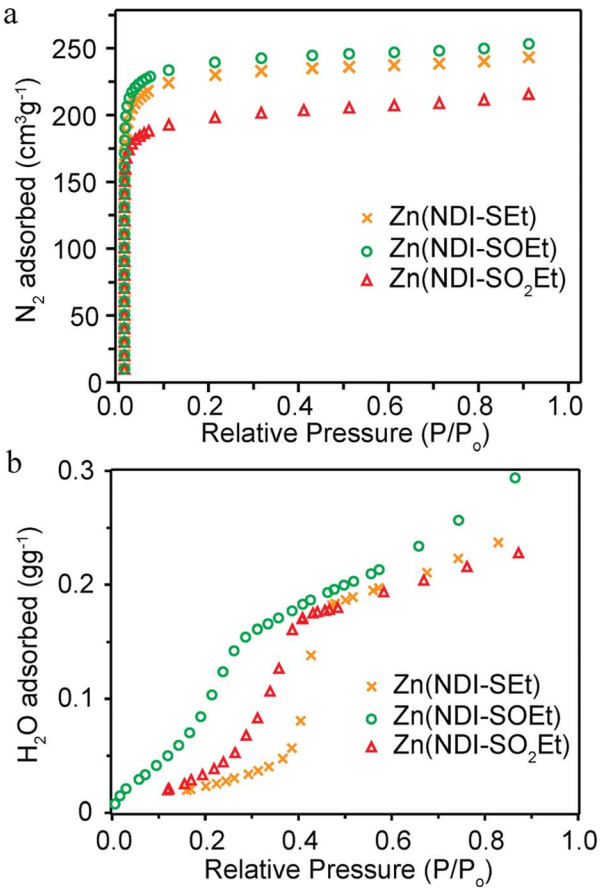

Fig. 5 (a) N_2 and (b) H_2O adsorption isotherms for Zn(NDI–SEt), Zn(NDI–SOEt), and Zn(NDI–SO_2Et) measured at 77 K and 293 K, respectively.

which water adsorption occurs at the adsorbent determines the minimum temperature for cooling, T_{evap}, and the maximum allowable adsorbent temperature, T_{ads}. In the present case, Zn(NDI–SEt), Zn(NDI–SOEt) and Zn(NDI–SO_2Et) experience steep adsorption steps just prior to P/P_o values of 0.466, 0.312, and 0.431, respectively. At these relative humidities, similar water loadings of 0.18, 0.16, and 0.17 g g^{-1} may be achieved. However, for a fixed T_{ads} of 40 °C, Zn(NDI–SEt), Zn(NDI–SOEt) and Zn(NDI–SO_2Et) should maintain different minimum cooling temperatures (T_{evap}) of 26.4 °C, 19.8 °C, and 25.1 °C, respectively, at these loadings (Table 1). Conversely, for a T_{evap} = 20 °C cooling application, these materials should be expected to most efficiently function as adsorbents at $T_{ads} \leq$ 32.9 °C, 40.3 °C, and 34.3 °C, respectively. Importantly, the calculated working temperatures achieved by these materials are all relevant for applications around room temperature and are achievable in a few synthetic steps from a unique parent material that is obtainable in large scale.

Table 1 Observed water loading lifts after initial water adsorption step and calculated minimum T_{evap} and maximum T_{ads} values based on the corresponding P/P_o values

	Lift (g g^{-1})	Min T_{evap}	Max T_{ads}
Zn–NDI–X	(@ P/P_o)	(T_{ads} = 40 °C)	(T_{evap} = 20 °C)
SEt	0.18 (0.466)	26.4 °C	32.9 °C
SOEt	0.16 (0.312)	19.8 °C	40.3 °C
SO_2Et	0.17 (0.431)	25.1 °C	34.3 °C

Conclusions

The foregoing results demonstrate the use of a modular synthetic approach to generate water stable and functional pyrazolate-based MOFs which may be postsynthetically modified to tune water adsorption characteristics. Such a strategy could be beneficial for implementing MOFs in water adsorption applications, such as adsorption heating and cooling processes, where the relative humidity at which water uptake occurs plays a major role in adsorbent and device performance. Furthermore, the materials described herein are constructed from benign Zn^{2+} and ligands which can be accessed in large scale through a modular synthetic approach, portending applications in real devices.

Acknowledgements

We gratefully acknowledge financial support for this research from the MIT Energy Initiative through a Seed Grant to MD. Grants from the NSF also provided instrument support to the DCIF at MIT (CHE-9808061, DBI-9729592). We thank Dr Shankar Narayanan and Prof. Evelyn Wang for valuable discussions.

Notes and references

1 R. Wang and R. Oliveira, *Prog. Energy Combust. Sci.*, 2006, **32**, 424–458.
2 H.-M. Henning, *Appl. Therm. Eng.*, 2007, **27**, 1734–1749.
3 A. Mahesh and S. C. Kaushik, *J. Renewable Sustainable Energy*, 2012, **4**, 022701.
4 K. C. Ng, H. T. Chua, C. Y. Chung, C. H. Loke, T. Kashiwagi, A. Akisawa and B. B. Saha, *Appl. Therm. Eng.*, 2001, **21**, 1631–1642.
5 J. Jänchen, D. Ackermann, H. Stach and W. Brösicke, *Sol. Energy*, 2004, **76**, 339–344.
6 S. K. Henninger, F. P. Schmidt and H.-M. Henning, *Adsorption*, 2011, **17**, 833–843.
7 S. K. Henninger, F. Jeremias, H. Kummer, P. Schossig and H.-M. Henning, *Energy Procedia*, 2012, **30**, 279–288.
8 A. Ristić, N. Z. Logar, S. K. Henninger and V. Kaučič, *Adv. Funct. Mater.*, 2012, **22**, 1952–1957.
9 L. Bonaccorsi, L. Calabrese, A. Freni and E. Proverbio, *Microporous Mesoporous Mater.*, 2013, **167**, 30–37.
10 P. Tatsidjodoung, N. Le Pierrès and L. Luo, *Renewable Sustainable Energy Rev.*, 2013, **18**, 327–349.
11 S. K. Henninger, F. P. Schmidt and H.-M. Henning, *Appl. Therm. Eng.*, 2010, **30**, 1692–1702.
12 S. K. Henninger, F. Jeremias, H. Kummer and C. Janiak, *Eur. J. Inorg. Chem.*, 2012, **2012**, 2625–2634.
13 M. P. Suh, H. J. Park, T. K. Prasad and D.-W. Lim, *Chem. Rev.*, 2012, **112**, 782–835.
14 T. A. Makal, J.-R. Li, W. Lu and H.-C. Zhou, *Chem. Soc. Rev.*, 2012, **41**, 7761–7779.

15 K. Sumida, D. L. Rogow, J. A. Mason, T. M. McDonald, E. D. Bloch, Z. R. Herm, T.-H. Bae and J. R. Long, *Chem. Rev.*, 2012, **112**, 724–781.
16 P. Küsgens, M. Rose, I. Senkovska, H. Fröde, A. Henschel, S. Siegle and S. Kaskel, *Microporous Mesoporous Mater.*, 2009, **120**, 325–330.
17 J. J. Low, A. I. Benin, P. Jakubczak, J. F. Abrahamian, S. A. Faheem and R. R. Willis, *J. Am. Chem. Soc.*, 2009, **131**, 15834–15842.
18 K. A. Cychosz and A. J. Matzger, *Langmuir*, 2010, **26**, 17198–171202.
19 P. M. Schoenecker, C. G. Carson, H. Jasuja, C. J. J. Flemming and K. S. Walton, *Ind. Eng. Chem. Res.*, 2012, **51**, 6513–6519.
20 S. K. Henninger, H. A. Habib and C. Janiak, *J. Am. Chem. Soc.*, 2009, **131**, 2776–2777.
21 N. Gargiulo, M. Imperatore, P. Aprea and D. Caputo, *Microporous Mesoporous Mater.*, 2011, **145**, 74–79.
22 J. Ehrenmann, S. K. Henninger and C. Janiak, *Eur. J. Inorg. Chem.*, 2011, **2011**, 471–474.
23 F. Jeremias, A. Khutia, S. K. Henninger and C. Janiak, *J. Mater. Chem.*, 2012, **22**, 10148–10151.
24 A. Khutia, H. U. Rammelberg, T. Schmidt, S. Henninger and C. Janiak, *Chem. Mater.*, 2013, **25**, 790–798.
25 H. J. Choi, M. Dincă, A. Dailly and J. R. Long, *Energy Environ. Sci.*, 2010, **3**, 117.
26 N. Masciocchi, S. Galli, V. Colombo, A. Maspero, G. Palmisano, B. Seyyedi, C. Lamberti and S. Bordiga, *J. Am. Chem. Soc.*, 2010, **132**, 7902–7904.
27 H. J. Choi, M. Dincă and J. R. Long, *J. Am. Chem. Soc.*, 2008, **130**, 7848–7850.
28 M. Tonigold, Y. Lu, A. Mavrandonakis, A. Puls, R. Staudt, J. Möllmer, J. Sauer and D. Volkmer, *Chem.–Eur. J.*, 2011, **17**, 8671–8695.
29 C. Pettinari, A. Tăbăcaru, I. Boldog, K. V. Domasevitch, S. Galli and N. Masciocchi, *Inorg. Chem.*, 2012, **51**, 5235–5245.
30 V. Colombo, C. Montoro, A. Maspero, G. Palmisano, N. Masciocchi, S. Galli, E. Barea and J. A. R. Navarro, *J. Am. Chem. Soc.*, 2012, **134**, 12830–12843.
31 Y. Lu, M. Tonigold, B. Bredenkötter, D. Volkmer, J. Hitzbleck and G. Langstein, *Z. Anorg. Allg. Chem.*, 2008, **634**, 2411–2417.
32 N. Sakai, J. Mareda, E. Vauthey and S. Matile, *Chem. Commun.*, 2010, **46**, 4225–4237.
33 K. K. Tanabe and S. M. Cohen, *Chem. Soc. Rev.*, 2011, **40**, 498–519.
34 S. M. Cohen, *Chem. Rev.*, 2012, **112**, 970–1000.
35 K. S. W. Sing, *Pure Appl. Chem.*, 1985, **57**, 603–619.
36 E.-P. Ng and S. Mintova, *Microporous Mesoporous Mater.*, 2008, **114**, 1–26.
37 T. Horikawa, N. Sakao, T. Sekida, J. Hayashi, D. D. Do and M. Katoh, *Carbon*, 2012, **50**, 1833–1842.
38 A. J. Leo, *Methods Enzymol.*, 1991, **202**, 544–591.
39 A. D. Burrows, C. G. Frost, M. F. Mahon and C. Richardson, *Chem. Commun.*, 2009, 4218–4220.
40 The calculated molar surface areas of Zn(NDI–SEt), Zn(NDI–SOEt) and Zn(NDI–SO_2Et) are 566 m^2 $mmol^{-1}$, 606 m^2 $mmol^{-1}$ and 510 m^2 $mmol^{-1}$, respectively. While the trend in N_2 accessible surface area for these materials is not in agreement with the degree of linker substitution, the differences are minor as seen by the ~17% maximum deviation between Zn(NDI–SOEt) and Zn(NDI–SO_2Et). The slight differences observed may be attributed to partial pore blockage in the Zn(NDI–SEt) parent material or changes in the orientation and ordering of the ethyl substituent within the channel upon oxidation of the sulfur atom.
41 M. H. Abraham, H. S. Chadha, G. S. Whiting and R. C. Mitchell, *J. Pharm. Sci.*, 1994, **83**, 1085–1100.
42 G. Caron, P. Gaillard, P.-A. Carrupt and B. Testa, *Helv. Chim. Acta*, 1997, **80**, 449–462.